On the energy efficiency of electric vehicles with multiple motors

DE FILIPPIS, Giovanni, LENZO, Basilio <http://orcid.org/0000-0002-8520-7953>, SORNIOTTI, Aldo, GRUBER, Patrick, SANNEN, Koen and DE SMET, Jasper

On the energy efficiency of electric vehicles with multiple motors

Giovanni De Filippis, Basilio Lenzo, Aldo Sorniotti*, Patrick Gruber
University of Surrey
Guildford, Surrey, GU2 7XH, United Kingdom
*Corresponding author: a.sorniotti@surrey.ac.uk

Koen Sannen, Jasper De Smet
Flanders MAKE
Lommel, B – 3920, Belgium

***Abstract*—Electric Vehicles (EVs) with multiple motors permit to design the steady-state cornering response by imposing reference understeer characteristics according to expected vehicle handling quality targets. To this aim a direct yaw moment is generated by assigning different torque demands to the left and right vehicle sides. The reference understeer characteristic has an impact on the drivetrain input power as well. In parallel, a Control Allocation (CA) strategy can be employed to achieve an energy-efficient wheel torque distribution generating the reference yaw moment and wheel torque. To the knowledge of the authors, for the first time this paper experimentally compares and critically analyses the potential energy efficiency benefits achievable through the appropriate set-up of the reference understeer characteristics and wheel torque CA. Interestingly, the experiments on a four-wheel-drive EV demonstrator show that higher energy savings can be obtained through the appropriate tuning of the reference cornering response rather than with an energy-efficient CA.**

Keywords—torque-vectoring; control allocation; cornering; energy consumption; understeer characteristic

I. INTRODUCTION

EVs with multiple motors allow the design of the cornering response through torque-vectoring strategies that generate a yaw moment, caused by different electric motor torques at the left and right wheels [1-4]. Hence, the same vehicle hardware can originate different understeer characteristics (i.e., the graphs of steering wheel angle, δ, as a function of lateral acceleration, a_Y, for steady-state conditions), depending on the tuning of the torque-vectoring controller.

At the same time, because of the influence of direct yaw moment control on the drivetrain power losses and tire slip power losses, the reference understeer characteristics have an impact on vehicle energy efficiency [5]. An extensive literature (for example, see [6-8]) discusses how EV energy efficiency can be improved by setting the most appropriate wheel torque distribution to achieve the overall reference traction force and yaw moment. However, to the knowledge of the authors there is an important gap in assessing and predicting the impact of the reference level of EV understeer (and hence of reference yaw rate and reference yaw moment) on energy efficiency.

Firstly, this study describes a CA strategy minimizing drivetrain power losses. The algorithm is validated along driving cycles executed on a rolling road facility, and through skid-pad tests. Secondly, the paper evaluates the power consumption corresponding to different reference understeer characteristics. The novel results permit an appreciation of the significance of the reference cornering response on the EV power input, and provide useful design guidelines for energy-efficient torque-vectoring controllers.

II. BACKGROUND

A. The vehicle demonstrator

The case study EV is the prototype Range Rover Evoque of the European Union FP7 project iCOMPOSE [9], with four identical on-board electric drivetrains, each of them consisting of a switched reluctance electric motor, a double-stage single-speed transmission system, constant velocity joints and a half-shaft. The vehicle demonstrator is shown in Fig. 1.

The simplified schematic of the vehicle control system is reported in Fig. 2. The control structure consists of three main layers:

i) A reference generator (Layer 1) responsible for defining the target values of the vehicle states (such as the reference yaw rate, r_{ref}) starting from the driver inputs (i.e., the steering wheel angle, δ, and the accelerator and brake pedal positions, p_a and p_b), and the measured or estimated vehicle states (e.g., vehicle speed, V, and longitudinal acceleration, a_X).

ii) A high-level controller (Layer 2) generating the overall traction/braking force and yaw moment demands, F_X^c and M_Z^c, to achieve the reference values of the vehicle states. M_Z^c is the yaw moment contribution caused by the torque-vectoring controller, i.e., by the difference among the wheel torques on the left- and right-hand sides of the vehicle. In particular, during the tests of this study the integral sliding mode controller described in [10] was adopted as yaw moment controller in Layer 2.

Fig. 1. The Range Rover Evoque vehicle demonstrator on the rolling road and during a cornering test.

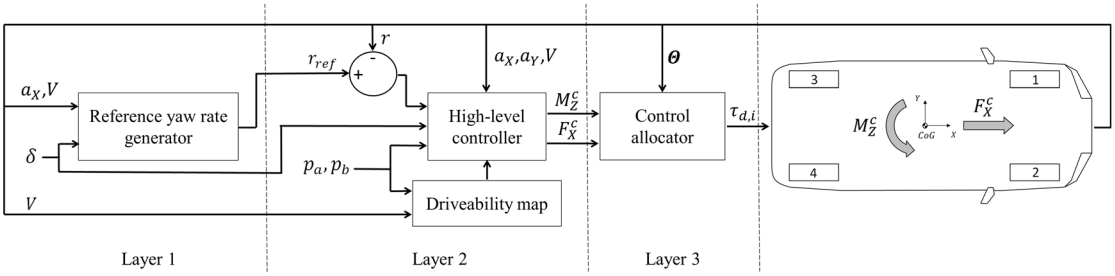

Fig. 2. Simplified schematic of the vehicle control system.

iii) A low-level controller (i.e., the 'Control allocator' in Fig. 2, Layer 3), which outputs the reference torques, $\tau_{d,i}$, for the individual wheels (see the numbering conventions in the figure), corresponding to the values of F_X^c and M_Z^c from the high-level controller in ii). $\boldsymbol{\theta}$ is the vector of parameters (the main one being vehicle speed) required for the calculation of the optimal wheel torque distribution (see [6]).

B. Energy-efficient control allocation

The energy-efficient CA strategy used in this study is based on the observation of the shape of the drivetrain power loss characteristics of the case study EV. They were measured on the MAHA rolling road facility available at Flanders MAKE (Belgium). The experimental characteristic of an individual drivetrain is shown in Fig. 3 as a function of the drivetrain torque demand (i.e., in a first approximation the electric motor torque demand multiplied by the transmission gear ratio), for different vehicle speeds. In traction the drivetrain power loss is defined as the difference between the measured electrical power at the inverter and the measured mechanical power at the roller of the rolling road. As a consequence, the measured power loss characteristics include the losses in the electric motor drive, mechanical transmission, tire rolling resistance and tire slip on the roller. The torque associated with drivetrain drag and tire rolling resistance was measured by applying zero torque demand to the electric motor drive, and imposing the desired level of wheel speed through the roller.

In this study, when the reference yaw moment defined in Layer 2 of the controller is assigned, the torque demand is split among the four drivetrains according to the energy-efficient CA algorithm described in [6] (unless otherwise specified). In particular, the control allocator calculates the torque demands for the left- and right-hand sides of the vehicle, respectively $\tau_{d,L}$ and $\tau_{d,R}$:

$$\tau_{d,L} = 0.5\left(F_X^c - \frac{M_Z^c}{d}\right)R$$
$$\tau_{d,R} = 0.5\left(F_X^c + \frac{M_Z^c}{d}\right)R \qquad (1)$$

with d being the half-track (assumed to be the same at the front and rear axles), and R the wheel radius. Two relatively simple CA problems are then solved independently, one for each vehicle side.

Based on the hypotheses (i.e., strictly monotonically increasing power loss characteristic with a single inflection point as a function of torque demand) and demonstration in [6], the CA strategy minimizing the drivetrain power losses in traction employs a single wheel on each side of the vehicle when the respective torque demand, $\tau_{d,L}$ or $\tau_{d,R}$, is lower than a switching value, $\tau_{d,SW}$. Vice versa, side torque demands greater than the switching threshold are evenly distributed between the two wheels on the same side. If the vehicle has four electric drivetrains with equal power loss characteristics, $P_{loss,i}$ (which is the case for the vehicle demonstrator in Fig. 1, in a first approximation), then $P_{loss,i}(\tau_{d,i}, \boldsymbol{\theta}) = P_{loss}(\tau_d, \boldsymbol{\theta})$. Thus, the value of $\tau_{d,SW}$ can be obtained off-line through the following equation:

$$P_{loss}(\tau_{d,SW}, \boldsymbol{\theta}) + P_{loss}(0, \boldsymbol{\theta}) = 2P_{loss}\left(\frac{\tau_{d,SW}}{2}, \boldsymbol{\theta}\right) \qquad (2)$$

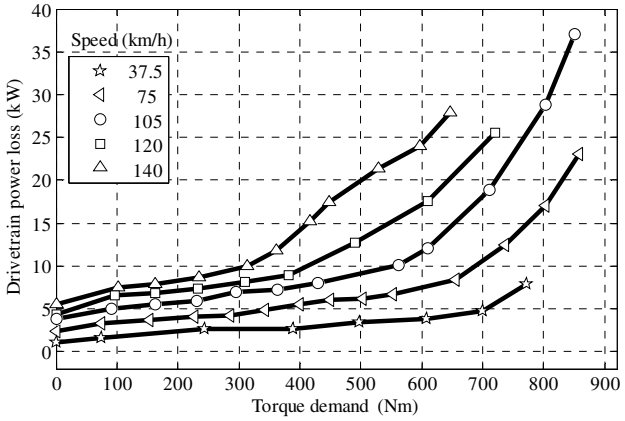

Fig. 3. Experimental power loss characteristics in traction for the left front electric drivetrain for different vehicle speeds.

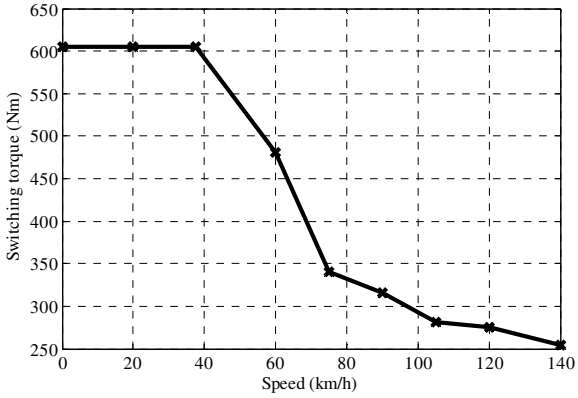

Fig. 4. Switching torques ($\tau_{d,SW}$) calculated at different vehicle speeds.

Similarly to the drivetrain power loss characteristics (Fig. 3), the switching torque depends on vehicle speed. In particular, Fig. 4 shows that for the specific vehicle $\tau_{d,SW}$

decreases as a function of speed. The markers in the figure indicate the vehicle speeds at which the switching torque was calculated.

The switching algorithm for energy-efficient CA can be implemented on the vehicle in the form of a look-up table. In practice, the transition between the single wheel and even distribution cases is smoothened by means of appropriate sigmoid functions, to prevent drivability issues. Moreover, in particular conditions, e.g. during medium-high braking and when the tire-road friction limits or the drivetrain torque limits are approached, the CA strategy is overruled by the electronic brake distribution algorithm, the individual wheel slip controllers or other safety-critical algorithms.

III. TEST PROCEDURES

A. Driving cycles for CA validation

For the purpose of CA validation, the vehicle demonstrator was tested on the rolling road along four driving cycles: i) the New European Driving Cycle (NEDC); ii) the Artemis Road driving cycle; iii) the Extra Urban Driving Cycle (EUDC, this cycle was run with an emulated uphill constant road slope of 8%); and iv) a newly introduced driving cycle, namely the Surrey Designed Driving Cycle (SDDC). The SDDC (Fig. 5) was conceived to emphasize the effect of CA on energy consumption. In fact, for the conventional driving cycles on a horizontal road, the torque distributions chosen by the presented CA algorithm tend to be close to the single-axle distribution. This behavior is due to the rather low torque demands and the very high power rating of the available electric motors installed on the demonstrator vehicle. In other words, an electric vehicle with less powerful drivetrains would not show this behavior, which also justifies the simulation of a road slope along the EUDC. The performances of the same electric vehicle were also analyzed when operating in a front-wheel-drive mode (Single Axle, SA), and in a four-wheel-drive mode (Even Distribution, ED) with constant 50:50 front-to-rear wheel torque distribution.

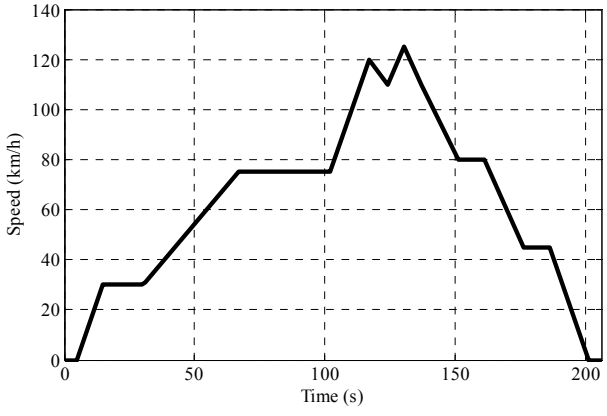

Fig. 5. Speed profile of the SDDC.

B. Skid-pads for CA validation

Skid-pad tests were executed at the Lommel proving ground (Belgium), on a circular path with 60 m radius, in order to validate the proposed CA strategy in cornering for high tire-road friction conditions. To quantify the benefits of the CA algorithm on its own with respect to the SA and ED modes, the vehicle was set in passive configuration, i.e., with reference yaw moment equal to zero.

C. Skid-pads for assessing the impact of vehicle understeer on energy consumption

To evaluate the effect of the reference understeer characteristic on its own in the skid-pad tests, the torque demands on each vehicle side were evenly distributed among the front and rear drivetrains (ED mode):

$$\tau_{d,1} = \tau_{d,3} = \frac{\tau_{d,L}}{2}$$
$$\tau_{d,2} = \tau_{d,4} = \frac{\tau_{d,R}}{2} \quad (3)$$

$\tau_{d,L}$ and $\tau_{d,R}$ were calculated on-line with Eq. (1), using the outputs of the high-level controller (Layer 2 in Fig. 2). The 60 m radius skid-pad tests were performed at four different values of a_y, i.e., ~2, 4, 6 and 8 m/s^2, by running the vehicle at speeds of ~39, 56, 68 and 79 km/h. The tarmac was dry during the whole session (i.e., to guarantee high tire-road friction values).

Fig. 6 reports the experimentally measured points of eleven understeer characteristics that were tested: the characteristic of the passive vehicle (denoted as PV), five characteristics with progressively increasing understeer (denoted as U1, U2, …, U5), and five characteristics with progressively decreasing understeer (denoted as O1, O2, …, O5) with respect to the passive vehicle. Typical for passenger vehicles, the PV is understeering, i.e., the required steering input increases with rising lateral acceleration. For the tests an appropriate formulation of the reference yaw rate in Layer 1 of the vehicle control system was implemented to achieve the reference understeer characteristics.

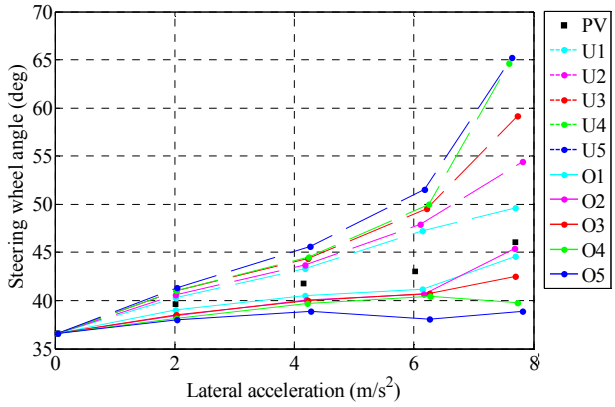

Fig. 6. The experimentally measured understeer characteristics.

D. Energy consumption measurement

During the tests, the energy consumption of the vehicle demonstrator, E, was calculated as the integral of the measured battery power output, P, along the relevant part of the test, defined by the time values t_{in} and t_{fin}:

$$E = \int_{t_{in}}^{t_{fin}} P\,dt = \int_{t_{in}}^{t_{fin}} V_{batt} I_{batt}\,dt \qquad (4)$$

where V_{batt} and I_{batt} are, respectively, battery voltage and current, measured with a TA057 Pico Technology voltage sensor and an HTR400-SB LEM current sensor.

IV. Results

A. CA effect along driving cycles

The experimental results related to the analyzed driving cycles are reported in Table I. In each operating condition, the adoption of the CA strategy leads to reduced energy consumption with respect to the SA and ED modes. For the NEDC and Artemis Road driving cycle the average torque demand level is moderate, and the optimal solution is very close to the SA mode. Therefore, the CA strategy provides a limited benefit with respect to the SA mode, and greater benefit with respect to the ED mode. For the EUDC the average torque demand is relatively high (because of the effect of the slope) and the optimal solution is very close to that of the ED mode. Consequently, the CA strategy provides a small improvement with respect to the ED mode, and greater improvement with respect to the SA mode. Over the SDDC, the CA algorithm is significantly better than the SA and ED modes.

TABLE I. Energy consumption along driving cycles

Driving cycle	Energy consumption (kWh)			Improvement (%) w.r.t.	
	SA	ED	CA	SA	ED
NEDC	2.932	3.031	2.923	0.31	3.56
Artemis Road	4.577	4.669	4.532	0.98	2.93
EUDC 8% slope	5.838	5.739	5.716	2.09	0.40
SDDC	1.136	1.141	1.103	2.90	3.33

B. CA effect during cornering

The measured average energy consumption values for a skid-pad lap are reported in Table II. At 2 and 6 m/s^2, the CA solution coincides with the single-axle on both vehicle sides. This is due to the fact that in steady-state cornering conditions, the overall traction force is limited. Energy savings of ~4% are achieved with respect to the ED mode.

TABLE II. Energy consumption for one skid-pad lap (60 m radius)

Lateral Acceleration (m/s^2)	Energy consumption (Wh)			Improvement (%) w.r.t.	
	SA	ED	CA	SA	ED
2	68.97	71.88	=SA	0	4.05
6	140.64	146.74	=SA	0	4.16

C. Effect of the understeer characteristic

Fig. 7 shows the average yaw moment demands, M_Z^c, generated by the yaw rate controller in Layer 2 as functions of a_Y, which were output by the integral sliding mode controller (see [10]) to track the reference yaw rate during the skid-pads. Positive yaw moments correspond to a destabilizing control action, i.e., less understeer, while negative yaw moments generate a stabilizing effect, i.e., more understeer.

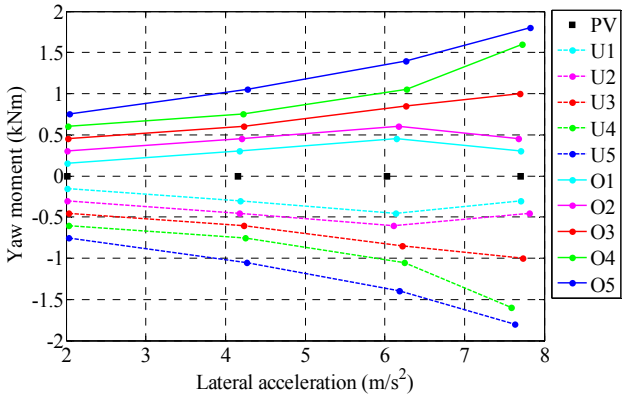

Fig. 7. Reference yaw moment as a function of lateral acceleration for different understeer characteristics.

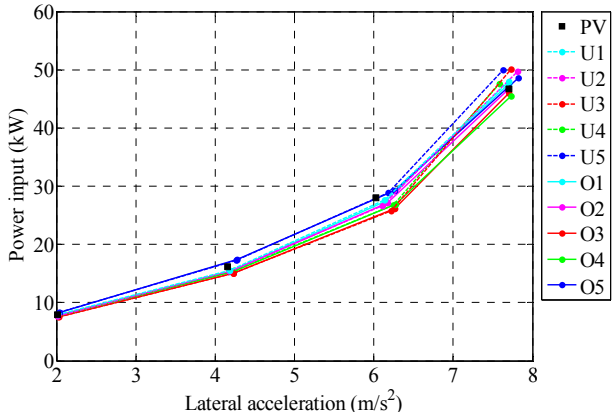

Fig. 8. Power input as a function of lateral acceleration for different understeer characteristics.

The average values of the measured input powers against a_Y are reported in Fig. 8. In general, the power input varies in a repeatable and significant manner with the reference yaw rate and understeer characteristic. However, from Fig. 8 it is difficult to distinguish the trends corresponding to the different reference cornering responses, as the variation of power input is not a monotonic function of the level of vehicle understeer.

As a consequence, the power consumptions of the experimentally measured points were plotted as functions of steering wheel angle and lateral acceleration (see Fig. 9). The experimental power input data were interpolated to obtain the map of the input power characteristic $P(a_Y, \delta) = V_{batt} I_{batt}$. The interpolated power profile was used to calculate the value of δ minimizing P for each assigned value of a_Y. In formulas:

$$\delta_{opt} = \arg min\, P(\delta)|_{a_Y = constant} \qquad (5)$$

The understeer characteristic corresponding to the minimum drivetrain power input, $\delta_{opt}(a_Y)$, is indicated in Fig. 9 with black solid circles. Fig. 9 also reports the iso-curves for the relative drivetrain power input increase (ΔP%, expressed in percentage) with respect to the optimal understeer

characteristic, $\delta_{opt}(a_Y)$ (see the contour curves at 5%, 9%, 13% and 17%, and the respective color bars).

The black squares indicate the understeer characteristic of the passive vehicle. Interestingly, the optimal understeer characteristic always implies less understeer with respect to the passive vehicle, and an overall cornering behavior close to neutral steering (i.e., with an approximately constant steering wheel angle regardless of the lateral acceleration value).

In comparison with the passive vehicle, the adoption of the optimal understeer characteristic allows energy savings of up to ~11%. For the case study vehicle these potential energy savings are even more significant than those achievable through the optimization of the CA algorithm (Layer 3 in Fig. 2, see Table I and Table II).

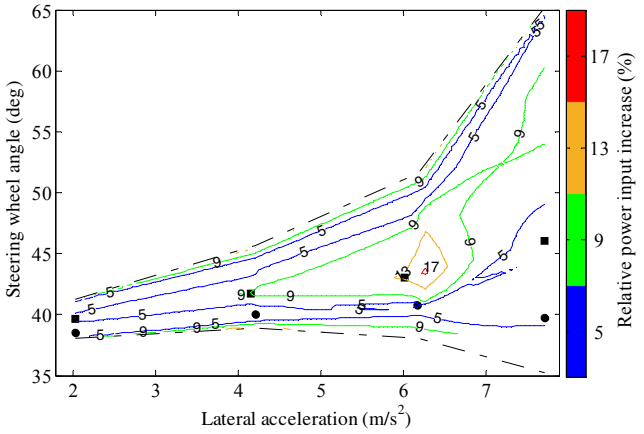

Fig. 9. $\Delta P\%$ (contour plots); optimal understeer characteristic (black solid circles); passive vehicle understeer characteristic (black solid squares); boundaries of the measured region (dash-dotted lines).

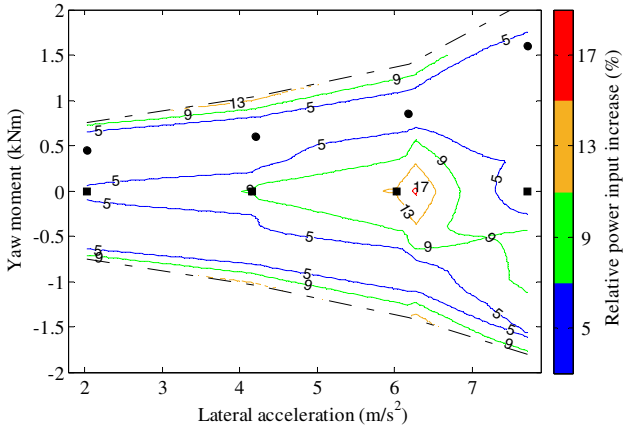

Fig. 10. $\Delta P\%$ (contour plots); optimal yaw moment characteristic (black solid circles); passive vehicle yaw moment characteristic (black solid squares); boundaries of the measured region (dash-dotted lines).

For completeness, Fig. 10 shows the $\Delta P\%$ contour plots on the graph of the reference yaw moment, M_Z^c, as a function of lateral acceleration, obtained with the same procedure as in Fig. 9. The black solid circles represents the yaw moment characteristic, $M_{Z,opt}^c(a_Y)$, corresponding to the minimum power input, i.e., the yaw moment giving origin to $\delta_{opt}(a_Y)$. $M_{Z,opt}^c$ is monotonically increasing with a_Y. For a given a_Y, starting from the lower bounds of M_Z^c, $\Delta P\%(M_Z^c)$ is characterized by:

i) A reduction as a function of M_Z^c, for low (negative) values of M_Z^c. For example, for $M_Z^c < 0$, if a_Y~6 m/s^2, $\Delta P\%$ decreases from more than 9% (at the lower bound of the measured region) to less than 5%, where a local minimum is reached;

ii) A progressive increase, which brings a local maximum of $\Delta P\%$ for M_Z^c values close to zero;

iii) A progressive reduction for relatively small positive values of M_Z^c, until $\Delta P\%$ goes to zero, thus reaching its absolute minimum at $M_{Z,opt}^c$;

iv) An increase for significantly positive values of M_Z^c, with $\Delta P\% > 9\%$ at the top boundary of the measured region.

The nearly symmetric behavior of the $\Delta P\%$ contour characteristics (even if the absolute minimum, i.e., $\Delta P\% = 0$, is always reached for $M_Z^c > 0$) with respect to the axis $M_Z^c = 0$ of Fig. 10 will be the subject of further investigations.

V. Conclusion

The presented experimental analysis allows the following conclusions:

- The energy-efficient CA algorithm brings energy savings typically between 2% and 3% along driving cycles with respect to fixed torque distribution strategies.
- In the measured cornering conditions, the energy-efficient CA allows energy consumption reductions of ~4% with respect to the ED mode.
- With a proper tuning of the reference cornering response, it is possible to obtain significant energy savings (higher than the savings obtainable with the CA) with respect to the passive vehicle. In particular, the optimal understeer characteristic brings measured input power reductions of up to ~11% for the case study vehicle demonstrator.
- The optimal understeer characteristic in terms of energy efficiency is close to the condition of neutral steering for the specific electric vehicle.
- For a given value of lateral acceleration, the pattern of the power loss variation as a function of the reference yaw moment is characterized by a relatively symmetric behavior, even if the absolute minimum is always achieved for destabilizing yaw moments.

References

[1] L. De Novellis, A. Sorniotti, P. Gruber, "Optimal wheel torque distribution for a four-wheel-drive fully electric vehicle," SAE International Journal of Passenger Cars – Mechanical Systems, vol. 6, pp. 128-136, 2013.

[2] K. Maeda, H. Fujimoto, Y. Hori, "Four-wheel driving-force distribution method based on driving stiffness and slip ratio estimation for electric vehicle with in-wheel motors," IEEE Vehicle Power and Propulsion Conference (VPPC), 2012.

[3] L. Feiqiang, W. Jun, L. Zhaodu, "Motor torque based vehicle stability control for four-wheel-drive electric vehicle," IEEE Vehicle Power and Propulsion Conference (VPPC), 2009.

[4] L. De Novellis, A. Sorniotti, P. Gruber, “Design and comparison of the handling performance of different electric vehicle layouts,” Proceedings of the Institution of Mechanical Engineers, Part D: Journal of Automobile Engineering, vol. 228, pp. 218-232, 2014.
[5] L. De Novellis, A. Sorniotti, P. Gruber, “Driving modes for designing the cornering response of fully electric vehicles with multiple motors,” Mechanical Systems and Signal Processing, vol. 64-65, pp. 1-15, 2015.
[6] A. M. Dizqah, B. Lenzo, A. Sorniotti, P. Gruber, S. Fallah, J. De Smet, “A Fast and Parametric Torque Distribution Strategy for Four-Wheel-Drive Energy Efficient Electric Vehicles,” IEEE Transactions on Industrial Electronics, vol. 63, pp. 4367-4376, 2016.
[7] X. Yuan, J. Wang, “Torque Distribution Strategy for a Front- and Rear-Wheel-Driven Electric Vehicle,” IEEE Transactions on Vehicular Technology, vol. 61, pp. 3365-3374, 2012.
[8] L. De Novellis, A. Sorniotti, P. Gruber, “Wheel Torque Distribution Criteria for Electric Vehicles with Torque-Vectoring Differentials,” IEEE Transactions on Vehicular Technology, vol. 63, pp. 1593-1602, 2014.
[9] http://www.i-compose.eu, last accessed on 25th May 2016.
[10] T. Goggia, A. Sorniotti, L. De Novellis, A. Ferrara, P. Gruber, J. Theunissen, J. Zehetner, “Integral Sliding Mode for the Torque-Vectoring Control of Fully Electric Vehicles: Theoretical Design and Experimental Assessment,” IEEE Transactions on Vehicular Technology, vol. 64, pp. 1701-1715, 2015.